21 May 2026

One Emitter, Many Lifetimes: Formulation-Encoded TADF Organic Dots for Multiplexed Imaging of Cancer-Immune Cell Co-Cultures

Janine Haug[1,2,3], Ferran Nadal-Bufi[4,5], André Jung[2], David B. Cordes[2], Aidan P. McKay[2], Olaf Fuhr[6], Marc Vendrell[4,5], Stefan Bräse[1,3], Eli Zysman-Colman[2]

1. Institute of Biological and Chemical Systems - Functional Molecular Systems, Karlsruhe Institute of Technology (KIT
2. Organic Semiconductor Centre, EaStCHEM School of Chemistry, University of St Andrews
3. Institute of Organic Chemistry, Karlsruhe Institute of Technology (KIT
4. Centre for Inflammation Research, University of Edinburgh
5. IRR Chemistry Hub, Institute for Regeneration and Repair, The University of Edinburgh
6. Institute of Nanotechnology (INT) and Karlsruhe Nano-Micro Facility (KNMFi, Karlsruhe Institute of Technology (KIT

Abstract

Thermally activated delayed fluorescence (TADF)-based organic dots (Odots) are an attractive class of luminescent probes for multiplexed fluorescence lifetime imaging microscopy (FLIM) as they can provide an unprecedented degree of tunability of their photoluminescence (PL) lifetimes. In this work, we demonstrate how formulation control of the Odot composition can be used to modulate the PL lifetime, which was then exploited in multiplexed FLIM studies. We synthesized and evaluated 48 TADF-Odots composed of eight structurally related derivatives of the multiresonant TADF (MR-TADF) emitter DiKTa, differing in number, strength, and steric demand of donor substituents, and six different formulations that modulated the degree of emitter aggregation. Controlled decrease in emitter aggregation as a function of doping concentration in the Odots produced a progressive blue-shift in the 1 emission, an increase in PL quantum yield up to 53%, and a lengthening of the PL lifetime, ultimately producing a family of Odots with PL lifetimes ranging from 4 to 35 ns. In vitro FLIM experiments in cancer cells validated the strategy for tuning the photophysics as a function of formulation, with PL lifetimes ranging from 3 to 16 ns. Finally, using different Odot formulations, each with the same emitter, we demonstrated signal resolution in multiplexed imaging experiments of co-cultures of human cancer and immune cells.

Posted on 21 May 2026 — CC-BY 4.0 — This is a preprint and has not been peer reviewed. Data may be preliminary. — https://doi.org/10.26434/chemrxiv.15003712/v1

Keywords

TADF, FLIM, nanoparticles, emission lifetime, imaging

Posted on 21 May 2026 — CC-BY 4.0 — This is a preprint and has not been peer reviewed. Data may be preliminary. — https://doi.org/10.26434/chemrxiv.15003712/v1

One Emitter, Many Lifetimes: Formulation-Encoded TADF Organic Dots for Multiplexed Imaging of Cancer-Immune Cell Co-Cultures

Janine Haug[a,b,c†], Ferran Nadal-Bufi[d,e†], André Jung[c], David B. Cordes[c], Aidan P. McKay[c], Olaf Fuhr[f], Marc Vendrell[d,e], Stefan Bräse[a,b]*, and Eli Zysman-Colman[c]**

[a] Institute of Biological and Chemical Systems - Functional Molecular Systems, Karlsruhe Institute of Technology (KIT), Kaiserstrasse 12, 76131 Karlsruhe, Germany. E-mail: braese@kit.edu

[b] Institute of Organic Chemistry, Karlsruhe Institute of Technology (KIT), Kaiserstrasse 12, 76131 Karlsruhe, Germany.

[c] Organic Semiconductor Centre, EaStCHEM School of Chemistry, University of St Andrews, St Andrews KY16 9ST, Fife, UK. E-mail: eli.zysman-colman@st-andrews.ac.uk

[d] Centre for Inflammation Research, The University of Edinburgh, EH16 4UU Edinburgh, UK. Email: marc.vendrell@ed.ac.uk

[e] IRR Chemistry Hub, Institute for Regeneration and Repair, The University of Edinburgh, EH16 4UU Edinburgh, UK.

f Institute of Nanotechnology (INT) and Karlsruhe Nano-Micro Facility (KNMFi), Karlsruhe Institute of Technology (KIT), Kaiserstrasse 12, 76131 Karlsruhe, Germany.

† These authors contributed equally.

Keywords: TADF, FLIM, nanoparticles, emission lifetime, imaging

Abstract

Thermally activated delayed fluorescence (TADF)-based organic dots (Odots) are an attractive class of luminescent probes for multiplexed fluorescence lifetime imaging microscopy (FLIM) as they can provide an unprecedented degree of tunability of their photoluminescence (PL) lifetimes. In this work, we demonstrate how formulation control of the Odot composition can be used to modulate the PL lifetime, which was then exploited in multiplexed FLIM studies. We synthesized and evaluated 48 TADF-Odots composed of eight structurally related derivatives of the multiresonant TADF (MR-TADF) emitter **DiKTa**, differing in number, strength, and steric demand of donor substituents, and six different formulations that modulated the degree of emitter aggregation. Controlled decrease in emitter aggregation as a function of doping concentration in the Odots produced a progressive blue-shift in the

emission, an increase in PL quantum yield up to 53%, and a lengthening of the PL lifetime, ultimately producing a family of Odots with PL lifetimes ranging from 4 to 35 ns. *In vitro* FLIM experiments in cancer cells validated the strategy for tuning the photophysics as a function of formulation, with PL lifetimes ranging from 3 to 16 ns. Finally, using different Odot formulations, each with the same emitter, we demonstrated signal resolution in multiplexed imaging experiments of co-cultures of human cancer and immune cells.

Introduction

The increasing demand for multiplexed bioimaging strategies has driven considerable interest in time-resolved fluorescence imaging.[1] Fluorescence lifetime imaging microscopy (FLIM) offers a powerful alternative to intensity-based fluorescence imaging by measuring the photoluminescence (PL) decay, creating spatially-resolved maps based on PL lifetimes (τ_{PL}).[2] However, conventional fluorophores commonly have lifetimes of under 5 ns, overlapping with cellular autofluorescence thereby impacting both signal-to-noise and multiplexing capabilities.[3-5] Therefore, imaging probes with PL lifetimes exceeding 5 ns that are biocompatible and can be excited by yellow to red light are needed to allow for effective multiplexed imaging readouts in biological systems.

TADF is a photophysical mechanism that describes a dual emission process wherein directly formed singlet excitons either direct emit or are competitively converted to triplets via intersystem crossing (ISC) and these then convert back to singlets via reverse intersystem crossing (RISC) with the aid of thermal energy before emission, a process that results in a delay of the emitted photon. This delay is controlled by the rate constants of ISC (k_{ISC}) and RISC (k_{RISC}), which are themselves a function of the spin-orbit coupling (SOC), the reorganization energy (λ), and the energy between the singlet and triplet states (ΔE_{ST}). The latter is proportional to the overlap integral between the frontier orbitals involved in the transition from the ground state to the excited state. Therefore, for ΔE_{ST} to decrease, the orbital overlap must decrease, typically from the highest occupied molecular orbital (HOMO) and the lowest unoccupied molecular orbital (LUMO). The most common emitter design to segregate the electron density of the HOMO and LUMO is a strongly twisted donor-acceptor architecture, as in this class of TADF compounds, the donor and acceptor moieties are weakly conjugated. However, a consequence of this molecular design is that the oscillator strength for the transition also decreases as this is proportional to the overlap, leading to compounds with moderate PL quantum yields (Φ_{PL}). Furthermore, there is also a relatively large λ in the excited state compared to the ground state of these long-range charge transfer (LRCT) emitters, which engenders a broad emission spectrum.[6]

However, a class of TADF compounds with bright, narrowband emission are multiresonant TADF (MR-TADF) emitters. These are p- and n-doped polyaromatic hydrocarbon compounds whose position elicits

an alternating electron density pattern that is inverted in the excited state that produces the required small ΔE_{ST} to enable TADF from a short-range charge transfer (SRCT) excited state. As the global electron density resides globally on the same atoms, the oscillator strength remains high, while their typically rigid structures controls the small λ, and narrowband emission is observed.[7] There are two major subclasses of MR-TADF materials: one where the n-dopants are boron atoms and one where the n-dopants are carbonyl groups. In 2019, Yuan *et al.* introduced the first example of this latter subclass, **QAO** (aka **DiKTa**), a compound containing a central nitrogen donor and two carbonyl groups as acceptors.[8] In dilute toluene solution, **DiKTa** emits at λ_{PL} of 466 nm with full-width at half maximum (FWHM) of 167 meV (32 nm). It has a moderately large ΔE_{ST} of 0.18 eV, sufficiently small for TADF to occur and is prone to aggregate, which leads to radiative loss channels. The emission color can be tuned via judicious decoration of the **DiKTa** core, in many cases without disrupting the SRCT emissive excited state.[6, 9, 10] Thus, the photophysical properties of MR-TADF compounds like **DiKTa** seem ideally suited for FLIM studies.

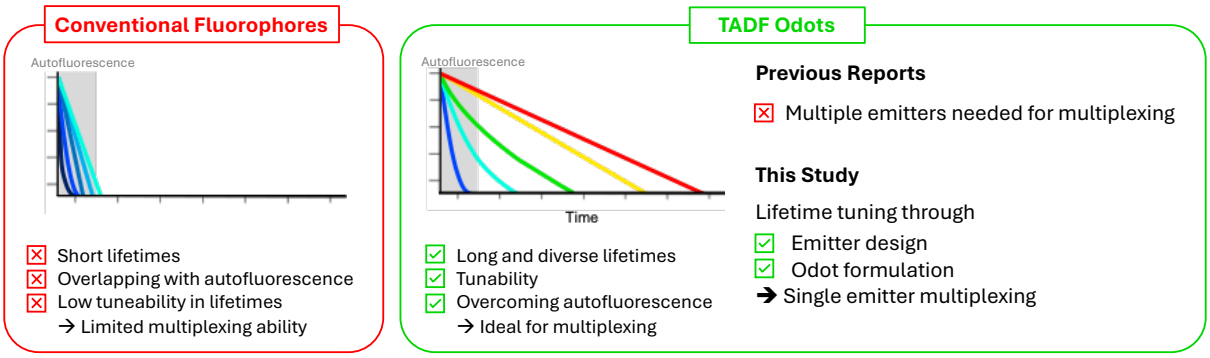


Figure **1**. TADF Odots over conventional fluorophores in multiplexed FLIM.

One main issue for the use of TADF emitters in biological applications is their poor solubility in aqueous media. Two main strategies have been developed to address this shortcoming: 1) molecular functionalization with hydrophilic groups;[11-13] or 2) formulation as nanoparticles via self-assembly[14-17] or encapsulation.[18-25] Notably, the latter requires amphiphilic surfactants that encapsulate the TADF emitter within a self-assembled, biocompatible micelle and no synthetic functionalization of the emitter is required.[26, 27] These organic dots (Odots) can be subdivided into aggregated Odots (*a*-Odots) that contain only the encapsulated emitter,[18-21] and glassy Odots (*g*-Odots) that are co-encapsulated emitter and host molecules, which have undergone a glass transition as a result of heating during Odot formation.[23, 24, 28-30] Because the degree of emitter aggregation within the Odot directly governs its photophysics (including Φ_{PL} and τ_{PL}), we envisaged that the formulation of Odots as a function of doping concentration could be leveraged for multiplexed FLIM imaging.

In the present work, we establish structure–formulation–property relationships in Odots and translate this insight to the multiplexed FLIM of cell co-cultures (**Error! Reference source not found.**). We have synthesized a family of eight **DiKTa**-based emitters decorated with *N*-heterocyclic donors of

varying strength, spatial demand, and substitution number. We formulated each of these emitters into six Odot compositions (i.e., neat *a*-Odots, *N*,*N*-dimethylethylenediamine (DMEDA)-containing Odots, and host:guest *h*-Odots using different doping ratios of the host 1,3-bis(*N*-carbazolyl)benzene (mCP), yielding a library of 48 Odots, which displayed an unprecedentedly broad range of lifetimes between 4 and 36 ns. Systematic photophysical characterization and FLIM imaging in human cancer cells revealed structure-formulation-property relationships, highlighting that the PL lifetime of the Odots is directly related to donor strength and the propensity for emitter aggregation within the Odot. Finally, we utilized this information to prepare formulations of a single TADF emitter for the discrimination of human cancer cells and immune cells in co-culture experiments.

Design and Synthesis of PL-Tunable TADF Emitters

To explore the influence of the donor strength, number, and steric bulkiness on the photophysical properties of the formulated Odots, we designed eight structurally related **DiKTa** derivatives (**3Cz-DiKTa**, **3DBZ-DiKTa**, **3TBZ-DiKTa**, **3DPA-DiKTa**, **3SPA-DiKTa**, **SPA-DiKTa**, **3DMAC-DiKTa**, and **3SAF-DiKTa**, Figure **2a**). These eight **DiKTa** derivatives emit between λ_{PL} of 529–664 nm, enabling a desired low energy emission for live-cell imaging. The emitters are grouped by donor strength (Figure **2b**), containing relatively weak (**3Cz-DiKTa**), moderate (**3DPA-DiKTa**, **3DBZ-DiKTa**, **3TBZ-DiKTa**, **3SPA-DiKTa**, **SPA-DiKTa**), and strong (**3DMAC-DiKTa**, **3SAF-DiKTa**) donor substituents.[6, 31] The strength of the donor not only modulates the energy of the emissive SRCT excited state, which is characteristic of MR-TADF emitters, but also introduces a low-lying long-range charge transfer (LRCT) excited state associated with the electronic coupling of the donor and acceptor motifs. The relative energies of these two states affect the emission envelope, Φ_{PL}, and τ_{PL}. The steric bulk of the donors (Figure **2b**) modulates the intermolecular distances, where bulkier donors can mitigate aggregation-caused quenching. Within the moderate donor series, spatial demand increases progressively from diphenylamine (**DPA**) through 10,11-dihydro-5*H*-dibenzo[*b*,*f*]azepine (**DBZ**) and 9*H*-tribenzo[*b*,*d*,*f*]azepine (**TBZ**) to *N*-phenyl-9,9'-spirobi[fluorene]-2-amine (**SPA**). Moreover, by replacing the methyl groups in 9,10-dihydro-9,9-dimethylacridine (**DMAC**) with a fluorene unit in 10*H*-spiro[acridine-9,9'-fluorene] (**SAF**), the intermolecular distance can likewise be modulated in this family of strong donors. This systematic variation in donor strength, steric demand, and substitution pattern provides a basis for interrogating how emitter structure impacts the properties of the formulated Odots, ultimately modulating τ_{PL}. Of the eight emitters, **SPA-DiKTa**, **3SPA-DiKTa**, and **3SAF-DiKTa** are new and were synthesized via Buchwald-Hartwig cross-coupling between the brominated **DiKTa** derivatives and the donors in yields ranging from 73–94% (Figure **S1**), while **3Cz-DiKTa**,[10] **3DPA-DiKTa**,[32] **3DBZ-DiKTa**,[25] **3TBZ-DiKTa**,[25] and **3DMAC-DiKTa**[10] were previously reported, and were synthesized following literature conditions. All emitters were characterized by ^{1}H NMR, ^{13}C NMR, and

2D NMR spectroscopy (Figures **S2**–**S7**), high-resolution mass spectrometry (Figures **S8**–**S10**), and infrared spectroscopy (Figures **S11**–**S13**). Single crystal X-ray diffraction studies confirmed the molecular structures of **3DBZ-DiKTa**, **3TBZ-DiKTa**, **SPA-DiKTa**, and **3SAF-DiKTa** (Figures **S14**–**17** and Tables **S1**–**S4**).

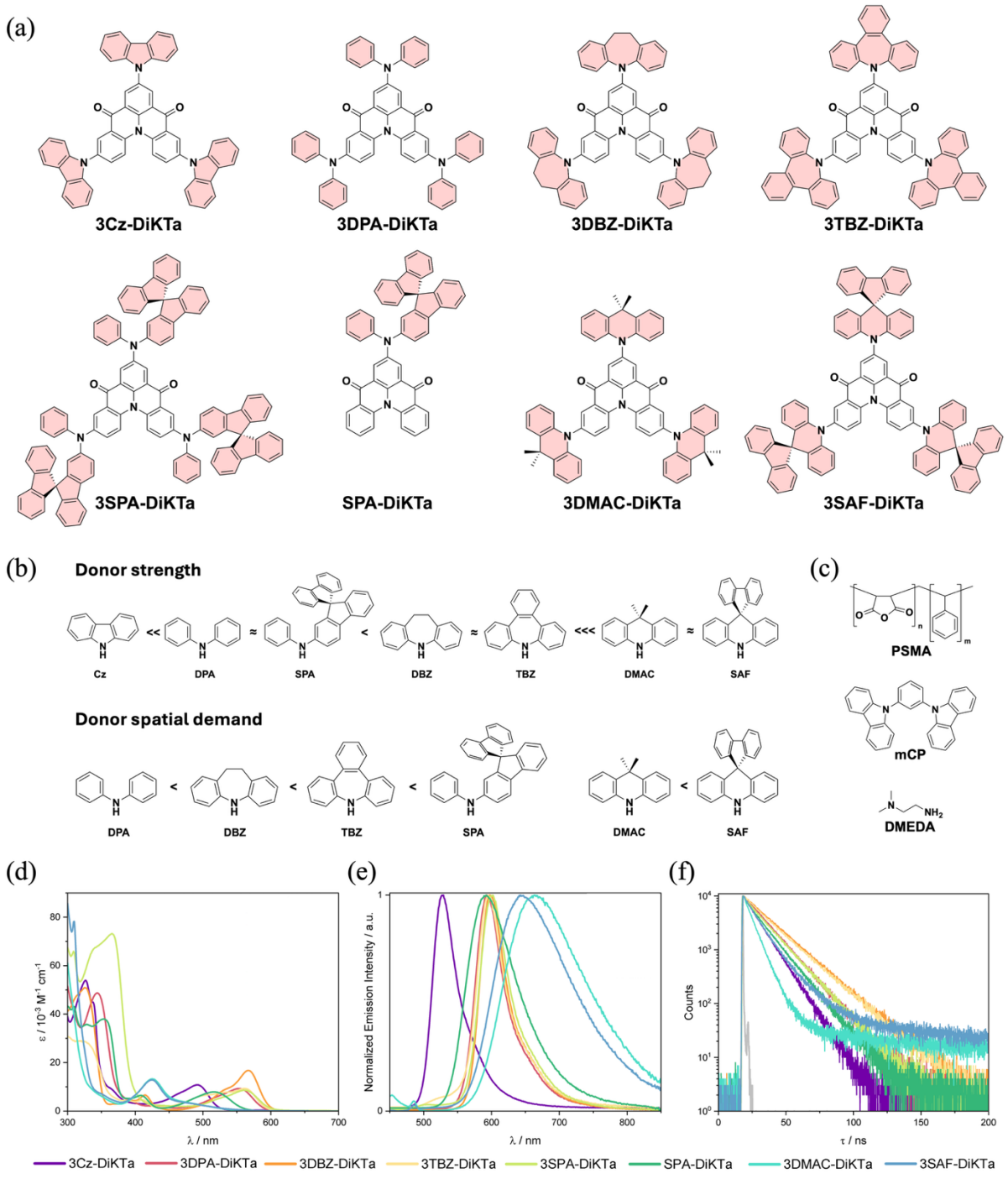


Figure **2**. (a) Chemical structures of the eight donor-decorated **DiKTa**-based TADF emitters. (b) Trends in donor strength (based on the HOMO energies, HOMO distribution, and donor geometries within the emitter) and spatial demand (based on the van der Waals volume of the trisubstituted emitters, Table **S5**, determined from either the ground-state optimized structures or the crystal structures) investigated

in this study. (c) Surfactant and additives employed in the preparation of Odots. (d) Absorption spectra, (e) PL spectra (λ_{exc} = 360 nm for **3Cz-DiKTa**, **3DPA-DiKTa**, **3SPA-DiKTa**, **SPA-DiKTa**; λ_{exc} = 414 nm for **3DBZ-DiKTa**, **3TBZ-DiKTa**; λ_{exc} = 424 nm for **3DMAC-DiKTa**, **3SAF-DiKTa**), and (f) PL decays of the emitters in dilute toluene solutions (λ_{exc} = 375 nm).

To provide a basis for the structure-property relationships, we first modelled the frontier molecular orbitals (FMOs) of the eight emitters at the PBE0/6-31G(d,p) level of theory in the gas phase (Table **S6** and Figure **S18**) for the ground state and at the RI-SCS-ADC(2)/cc-pVDZ level of theory for the excited states (Table **S6** and Figure **S20**).[33-35] In all eight emitters, the LUMO is localized on the **DiKTa** core, while the location of the HOMO varies depending on the donor strength. Emitters with weak-to-moderate donors have HOMOs that are delocalized across the **DiKTa** core and onto the donors. Emitters with strong donors or derivatives that are monosubstituted have HOMOs localized only on the donor. Donor substitution leads to a destabilized HOMO relative to the parent **DiKTa** (-6.21 eV), which is particularly pronounced upon trisubstitution with donors of moderate strength (HOMO energies of -5.00 to -4.77 eV). The HOMO is progressively stabilized moving from monosubstitution (-5.14 eV) and trisubstitution with strong donors (-5.26 to -5.40 eV) towards weak donors (-5.67 eV). The enhanced destabilization of the emitters with moderate donor strength compared to those with strong donors is likely due to the enhanced conjugation of the moderate donors into the acceptor (Figure **S18**). The LUMO energies of the emitters with moderate donors (-1.70 to -2.21 eV) are destabilized compared to those with strong donors (-2.62 to -2.68 eV). The resulting HOMO-LUMO gaps of all emitters (2.64 to 3.07 eV) are smaller compared to that of **DiKTa** (3.92 eV).

Due to the increased computational demand of the large emitters **3SPA-DiKTa** and **3SAF-DiKTa**, model compounds were computed at the RI-SCS-ADC(2)/cc-pVDZ level where the spirofluorene unit was replaced with a *gem*-dimethyl group, yielding **3SPAMe-DiKTa** (Figure **S19**) and **3DMAC-DiKTa**, respectively. The energies of the first excited singlet (S_1) and triplet (T_1) states of the eight compounds are stabilized compared to those of **DiKTa** (S_1 of 3.24 eV, T_1 of 2.97 eV), having comparable S_1 energies (2.36–2.54 eV), save for **3Cz-DiKTa** (with the weakest donor), whose S_1 energy is 2.71 eV. The T_1 states of **3DBZ-DiKTa**, **3TBZ-DiKTa**, **3DPA-DiKTa**, **3SPA-DiKTa**, and **SPA-DiKTa** have similar energies in the range of 2.13–2.34 eV, while **3Cz-DiKTa** and **3DMAC-DiKTa** possess higher-lying T_1 states at 2.50 and 2.46 eV, respectively.

The eight emitters can be divided into two groups based on the magnitude of the ΔE_{ST}: 1) emitters with weak and moderate donors as well as monosubstituted derivatives have ΔE_{ST} ranging between 0.20–0.30 eV, values that are comparable to other **DiKTa**-type MR-TADF materials;[6] and 2) **3DMAC-DiKTa**, an emitter with strong donors, has a very small ΔE_{ST} of 0.02 eV. The emitters can similarly be grouped based on the magnitude of the oscillator strength (*f*) for the S_0-S_1 transition, which is moderate (0.14–0.16) for the trisubstituted emitters bearing weak and moderate donors and is much smaller for **SPA-DiKTa**, reaching near-zero for **3DMAC-DiKTa** and **3SAF-DiKTa**. Thus, one group of emitters,

containing weak-to-moderate donors, has low-lying excited states of SRCT character, while the group of emitters with strong donors or that are monosubstituted has low-lying excited states with substantial LRCT character.

The photophysical properties of the eight emitters were first characterized in dilute toluene solution (Table **1**). Absorption spectra (Figure **2d**) show low-lying bands that progressively red-shift with increasing donor strength in the series of trisubstituted emitters from **3Cz-DiKTa** (λ_{abs} of 492 nm) to λ_{abs} of 553 to 566 nm for the moderate-donor series, with **3DBZ-DiKTa** showing the most red-shifted absorption. The absorption spectrum of monosubstituted analogue **SPA-DiKTa** (λ_{abs} of 516 nm) is blue-shifted compared to the trisubstituted **3SPA-DiKTa** (λ_{abs} of 561 nm). The absorption spectra of emitters with strong donors, **3DMAC-DiKTa** and **3SAF-DiKTa**, deviated significantly, featuring an intense absorption band near λ_{abs} of 425 nm with a low absorptivity tail extending to around 580 nm.

The PL spectra are shown in Figure **2e**. **3Cz-DiKTa** emits at λ_{PL} of 529 nm, while **3DPA-DiKTa**, **3DBZ-DiKTa**, **3TBZ-DiKTa**, and **3SPA-DiKTa** emit similarly at λ_{PL} between 592–602 nm. **3DMAC-DiKTa** and **3SAF-DiKTa** show the most red-shifted emission (λ_{PL} of 643 and 664 nm, respectively) as these compounds have the strongest donors. The emitters trisubstituted with weak-to-moderate donors displayed small Stokes shifts, narrowband emission with FWHM of 44 to 61 nm (172 to 208 meV) and moderate-to-good Φ_{PL} of 44–75%. Emission broadening was observed for **SPA-DiKTa** (FWHM of 87 nm or 298 meV) as well as **3DMAC-DiKTa** and **3SAF-DiKTa** (136 and 130 nm or 364 and 378 meV, respectively), with the latter two not showing the mirror image profile between absorption and emission spectra. The Φ_{PL} is 23% for **SPA-DiKTa**, while the values of **3DMAC-DiKTa** and **3SAF-DiKTa** were too low to be determined. PL solvatochromism studies (Figure **S21**) confirmed the SRCT character of the weak and moderate-donor series, the increased admixture of the LRCT character in the monosubstituted **SPA-DiKTa**, and the pronounced LRCT character of **3DMAC-DiKTa** and **3SAF-DiKTa**. Measured ΔE_{ST} values align well with the computed ones, with emitters with weak and moderate donors having ΔE_{ST} in the range of 0.12–0.24 eV, while emitters with strong donors have near-zero ΔE_{ST} (Figure **S22**). The ΔE_{ST} of all eight emitters are sufficiently small to enable TADF.[6] These measurements collectively imply that **3Cz-DiKTa**, **3DPA-DiKTa**, **3DBZ-DiKTa**, **3TBZ-DiKTa**, and **3SPA-DiKTa** emit from a SRCT state, while **SPA-DiKTa**, **3DMAC-DiKTa** and **3SAF-DiKTa** emit from a mixed SRCT/LRCT state, with the latter two featuring an increased admixture of the LRCT state, aligning well with the calculations. The time-resolved PL measurements of all emitters, except for **3DMAC-DiKTa** and **3SAF-DiKTa**, show monoexponential decay kinetics, with τ_{PL} ranging from 11.1 to 19.3 ns. The PL of **3DMAC-DiKTa** and **3SAF-DiKTa** decays with multiexponential kinetics, with prompt fluorescence lifetimes, τ_p, of 6.8 and 10.8 ns, respectively, and much slower delayed fluorescence lifetimes, τ_d, of 182 and 147 ns, respectively (Figure **2f**).

Having established the photophysical properties of monomolecular species, we next turned our attention to spin-coated film measurements of 2 wt% emitter doped in 1,3-bis(*N*-carbazolyl)benzene (mCP) to provide insight into the photophysical behavior of the host:guest system present within the *h*-Odots (Table **1**). The PL spectra of all emitters are red-shifted relative to toluene solution (Figure **S23**), consistent with increased polarity of the mCP host stabilizing the CT excited state. There is an unexpected blue-shift of the emission of **3DMAC-DiKTa** and **3SAF-DiKTa** from λ_{PL} of 664 and 643 nm in toluene to 598 and 595 nm in the 2 wt% doped film, which likely implies different conformations adopted in the film for these two emitters. **3Cz-DiKTa** has the highest Φ_{PL} of 84%, while **3DPA-DiKTa**, **3SPA-DiKTa**, and **SPA-DiKTa** showed comparable moderate values of between 52–56%. The Φ_{PL} of four emitters notably drop upon exposure to air to 44–68%, indicative of triplet-state quenching by molecular oxygen that is consistent with TADF emission. The Φ_{PL} of **3DBZ-DiKTa**, **3TBZ-DiKTa**, **3SAF-DiKTa**, and **3DMAC-DiKTa** are lower, ranging from 24–38%, which remain essentially unchanged on exposure to air.

Time-resolved PL measurements of the doped films reveal complex multiexponential decay kinetics, with both τ_p and τ_d each modelled as biexponential decays (Figure **S24**–**S26**, Table **S7**). This is not unusual given the inhomogeneous environment of the amorphous film. The $\tau_{p,\ avg}$ of the emitters trisubstituted with weak-to-moderate donors (**3Cz-DiKTa**, **3DPA-DiKTa**, **3DBZ-DiKTa**, **3TBZ-DiKTa**, and **3SPA-DiKTa**) range between 11.3 and 20.9 ns, showing no significant changes compared to the values in toluene solution. The $\tau_{p,\ avg}$ of the monosubstituted emitter **SPA-DiKTa** at 21.6 ns is much longer than the 13.7 ns in solution. The longest $\tau_{p,\ avg}$ are associated with emitters bearing strong donors, reaching up to 39.6 ns for **3SAF-DiKTa**. By contrast, **3DMAC-DiKTa** and **3SAF-DiKTa** have shorter $\tau_{d,\ avg}$ of 13.3 and 5.5 μs, respectively. The $\tau_{d,\ avg}$ of **3Cz-DiKTa** is two-orders of magnitude slower at 598 μs, while the $\tau_{d,\ avg}$ of **3DPA-DiKTa**, **3DBZ-DiKTa**, **3TBZ-DiKTa**, and **3SPA-DiKTa** are in in the millisecond regime, ranging between 6.2 and 26.9 ms. Similar to the trend in prompt lifetime, monosubstituted **SPA-DiKTa** has a longer $\tau_{d,\ avg}$ of 20.6 ms than **3SPA-DiKTa** ($\tau_{d,\ avg}$ of 11.8 ms). The singlet and triplet energies and by extension the ΔE_{ST} values in the doped film align well with those in solution (Table **1**, Figure **S27**). With a diversity of suitably long PL lifetimes, these film measurements establish the photophysical potential for *h*-Odots and set the stage for evaluating how nanoconfinement within *h*-Odots modulates these properties under biologically relevant conditions.

Table **1**. Summary of the photophysical properties in dilute solutions and 2 wt% doped films in mCP.

Emitter		λ_{abs} (ε) / nm (× 10^3 M^{-1} cm^{-1})	λ_{PL} / nm	FWHM / meV (nm)	Φ_{PL} / %	τ_p / ns	$\tau_{d,\ avg}$	S_1 / T_1 / eV	ΔE_{ST} / eV
3Cz-DiKTa	Sol.	492 (11) [a]	529 [a]	192 (44) [a]	44 [c]	11.1 [e]	-	2.49 / 2.28 [h]	0.21 [h]
	Film	-	538 [b]	218 (52) [b]	84 (68) [d]	11.3 [avg, f]	598 μs [g]	2.44 / 2.27 [j]	0.17 [j]
3DPA-DiKTa	Sol.	553 (9) [a]	593 [a]	173 (50) [a]	61 [c]	15.2 [e]	-	2.14 / 2.02 [h]	0.12 [h]
	Film	-	617 [b]	183 (57) [b]	56 (48) [d]	16.6 [avg, f]	6.2 ms [g]	2.06 / 1.96 [j]	0.13 [j]

3DBZ-DiKTa	Sol.	566 (17) [a]	598 [a]	208 (61) [a]	75 [c]	19.6 [e]	-	2.15 / 1.93 [i]	0.22 [i]
	Film	-	625 [b]	190 (60) [b]	38 (42) [d]	20.9 [f]	26.9 ms [g]	2.04 / 1.83 [j]	0.21 [j]
3TBZ-DiKTa	Sol.	562 (10) [a]	595 [a]	200 (58) [a]	65 [c]	19.3 [e]	-	2.12 / 1.83 [i]	0.29 [i]
	Film	-	611 [b]	178 (58) [b]	24 (24) [d]	20.6 [f]	18.6 ms [g]	2.07 / 1.89 [j]	0.18 [j]
3SPA-DiKTa	Sol.	561 (9) [a]	602 [a]	172 (51) [a]	48 [c]	15.6 [e]	-	2.14 / 1.95 [h]	0.19 [h]
	Film	-	616 [b]	190 (59) [b]	54 (44) [d]	17.6 [avg. f]	11.8 ms [g]	2.11 /1.99 [j]	0.12 [j]
SPA-DiKTa	Sol.	516 (8) [a]	592 [a]	298 (87) [a]	23 [c]	13.7 [e]	-	2.29 / 2.05 [h]	0.24 [h]
	Film	-	599 [b]	286 (86) [b]	52 (46) [d]	21.6 [avg. f]	20.6 ms [g]	2.24 / 2.02 [j]	0.22 [j]
3DMAC-DiKTa	Sol.	425 (13) [a]	664 [a]	364 (136) [a]	- [c]	6.8 [e]	182 ns [e]	2.32 / 2.32 [i]	≤ 0.01 [i]
	Film	-	598 [b]	350 (104) [b]	28 (26) [d]	27.7 [avg. f]	13.3 µs [g]	2.29 / 2.29 [j]	< 0.01 [j]
3SAF-DiKTa	Sol.	424 (13) [a]	643 [a]	378 (130) [a]	- [c]	10.8 [e]	147 ns [e]	2.34 / 2.34 [i]	≤ 0.01 [i]
	Film	-	595 [b]	368 (110) [b]	37 (35) [d]	39.6 [avg. f]	5.5 µs [g]	2.35 / 2.35 [j]	< 0.01 [j]

[a] In dilute toluene at 300 K (10^{-5} M; for PL: λ_{exc} = 360 nm for **3Cz-DiKTa**, **3DBZ-DiKTa**, **3TBZ-DiKTa**, **3DPA-DiKTa**, **3SPA-DiKTa**, **SPA-DiKTa**; λ_{exc} = 424 nm **3DMAC-DiKTa**, and **3SAF-DiKTa**). [b] In 2 wt% film in mCP (λ_{exc} = 340 nm). [c] Relative Φ_{PL} in solutions were measured by a comparative method using quinine sulfate as a standard (Φ_{PL} = 54.6% in 1 M H_2SO_4, λ_{exc} = 340 nm) for **3Cz-DiKTa** and rhodamine 6G as standard (Φ_{PL} = 95% in 10^{-5} M EtOH; λ_{exc} = 530 nm) for all other emitters. [d] Absolute Φ_{PL} of the 2 wt% films in mCP were measured using an integrating sphere (λ_{exc} = 340 nm). [e] In degassed dilute toluene solution (10^{-5} M), measured by TCSPC λ_{exc} = 375 nm. [f] In 2 wt% mCP film, measured by TCSPC (λ_{exc} = 375 nm). [g] In 2 wt% mCP film, measured by MCS (λ_{exc} = 340 nm). [h] Determined from the onsets of the SS PL and delayed emission spectra in 2-MeTHF 77 K (λ_{exc} = 360 nm). [i] Determined from the onsets of the SS PL and delayed emission spectra in toluene at 77 K (λ_{exc} = 360 nm). [j] Determined from the onsets of the SS-PL and phosphorescence spectra in 2 wt% mCP films at 77 K.

Optimizing Biocompatible Formulations of TADF Odots

We assessed the impact of six distinct formulations for all eight TADF emitters as a handle to modulate the photophysics of the Odots, producing neat *a*-Odots (*a* for aggregated), DMEDA-Odots (1:1 DMEDA:emitter), and host:guest *h*-Odots at four doping ratios (2–50 wt% in mCP). DMEDA (Figure ***2*c**) as an additive was used to introduce a positive charge to the Odot under physiological conditions. Poly(styrene-co-maleic anhydride) (PSMA, Figure **2c**) was used as the common surfactant, and mCP was employed as the host in the *h*-Odots (Figure **2c**). All Odots were prepared by nanoprecipitation,[25] yielding a collection of 48 TADF Odots whose photophysics were characterized in aqueous solutions (Figure **3** and Table **S8**).

Regardless of the Odots, absorption maxima did not vary as a function of formulation, and the spectra closely resembled those in toluene (Figure **S28**). The use of the mCP host in the *h*-Odots, especially at low doping concentration of emitter, effectively decreased the formation of aggregates, evident from progressively blue-shifted emission maxima compared to the *a*-Odot and increased Φ_{PL} as the doping level of the emitter decreased (Figure **3a** and **3b**). Notably, the PL spectra of the 2 wt% *h*-Odots closely match those of the 2 wt% doped films in mCP (Figure **3a** and Figure **S30**). The **3Cz-DiKTa** 2 wt% *h*-Odots emit in the green-to-yellow region, while all others in this series emit in the orange-to-red region, with those of **3DMAC-DiKTa** and **3SAF-DiKTa** display the broadest emission bands. For all emitters,

at least one *h*-Odot formulation has a Φ_{PL} exceeding 10%, with the 2 wt% *h*-Odot of **3Cz-DiKTa** having the highest Φ_{PL} of 53% (Figure **3b**); the 2 and 20 wt% *h*-Odots of **3DMAC-DiKTa** and **3SAF-DiKTa**, respectively, have the lowest Φ_{PL} among this family of only 13%. Irrespective of emitter, DMEDA-Odots have lower Φ_{PL} than 50 wt% *h*-Odots and similar Φ_{PL} to the *a*-Odots. These results are consistent with severe aggregation-caused quenching in the absence of a dispersing medium and are likely attributable to the higher concentrations of emitter present in the DMEDA-Odots compared to the 50 wt% *h*-Odots. Overall, Odots with low energy absorption bands and yellow-to-red emission spectra are desired as these would reduce overall toxicity and stress of biological samples and ensure compatibility with commonly employed FLIM setups. This combination of photophysical behavior is present for the Odots based on **3Cz-DiKTa**, **3DBZ-DiKTa**, **3TBZ-DiKTa**, **3DPA-DiKTa**, and **3SPA-DiKTa**. **SPA-DiKTa**, **3DMAC-DiKTa**, and **3SAF-DiKTa** show increased Stokes shifts, requiring relatively higher energy excitation to access their desirable red emission.

Dynamic light scattering (DLS) measurements revealed average diameters of 17–33 nm with polydispersity indices between 0.1–0.3 (Figure **S34** and Table **S8**). No trends in size or polydispersity between different emitters and formulations were observed, although polydispersity was generally higher for the DMEDA-Odots compared to other formulations. Scanning electron microscopy performed with all Odot formulations of **3DPA-DiKTa** as a prototypical case showed spherical morphologies and similar size distributions between most formulations (Figure **S35**). The photostability of the Odots was assessed under continuous 300 nm excitation for 10 min, with ≥ 90% retained PL intensity adopted as the benchmark (Figure **S33** and Table **S8**). Most Odots met this threshold; however, *h*-Odots of trisubstituted emitters with moderate donors (**3DBZ-DiKTa**, **3TBZ-DiKTa**, **3DPA-DiKTa**, **3SPA-DiKTa**, and **SPA-DiKTa**) showed PL bleaching.

Time-resolved PL measurements of the Odots revealed a prompt PL decay with average lifetimes ranging from 4.1 to 35.7 ns (Figure **3c** and **3d**, Figure **S31**). All Odot formulations with **3DMAC-DiKTa** and **3SAF-DiKTa** have an additional microsecond-long delayed PL lifetime (Figure **3e**, Figure **S32**, Table **S9**). The PL lifetimes of the *h*-Odots could be fitted to a biexponential function, while the PL lifetimes of the *a*- and DMEDA-Odots were better modelled to a triexponential decay kinetics, reflecting a greater heterogeneity of environment and speciation. Aligned with the observed increase in Φ_{PL} with decreasing emitter doping in the *h*-Odots, τ_{PL} increased systematically across all emitters, specifically from ~10 ns at 50 wt% to >20 ns at 2 wt% doping. DMEDA-Odots and 50 wt% *h*-Odots showed comparable τ_{PL} values across the series. The $\tau_{d,\,avg}$ of **3DMAC-DiKTa** and **3SAF-DiKTa** increased upon emitter dilution in the presence of the mCP host, from ~700–790 ns in the *a*- and DMEDA-Odots to 1,253 and 2,187 ns in the 2 wt% *h*-Odots with **3DMAC-DiKTa** and **3SAF-DiKTa**, respectively. This behavior is due to aggregation-caused quenching. In general, the delayed lifetimes are shortened compared to the films, potentially due to increased quenching by the encapsulated oxygen

within the Odot. Overall, these results demonstrate that formulation of the Odots enables systematic tuning of τ_{PL} irrespective of the emitter.

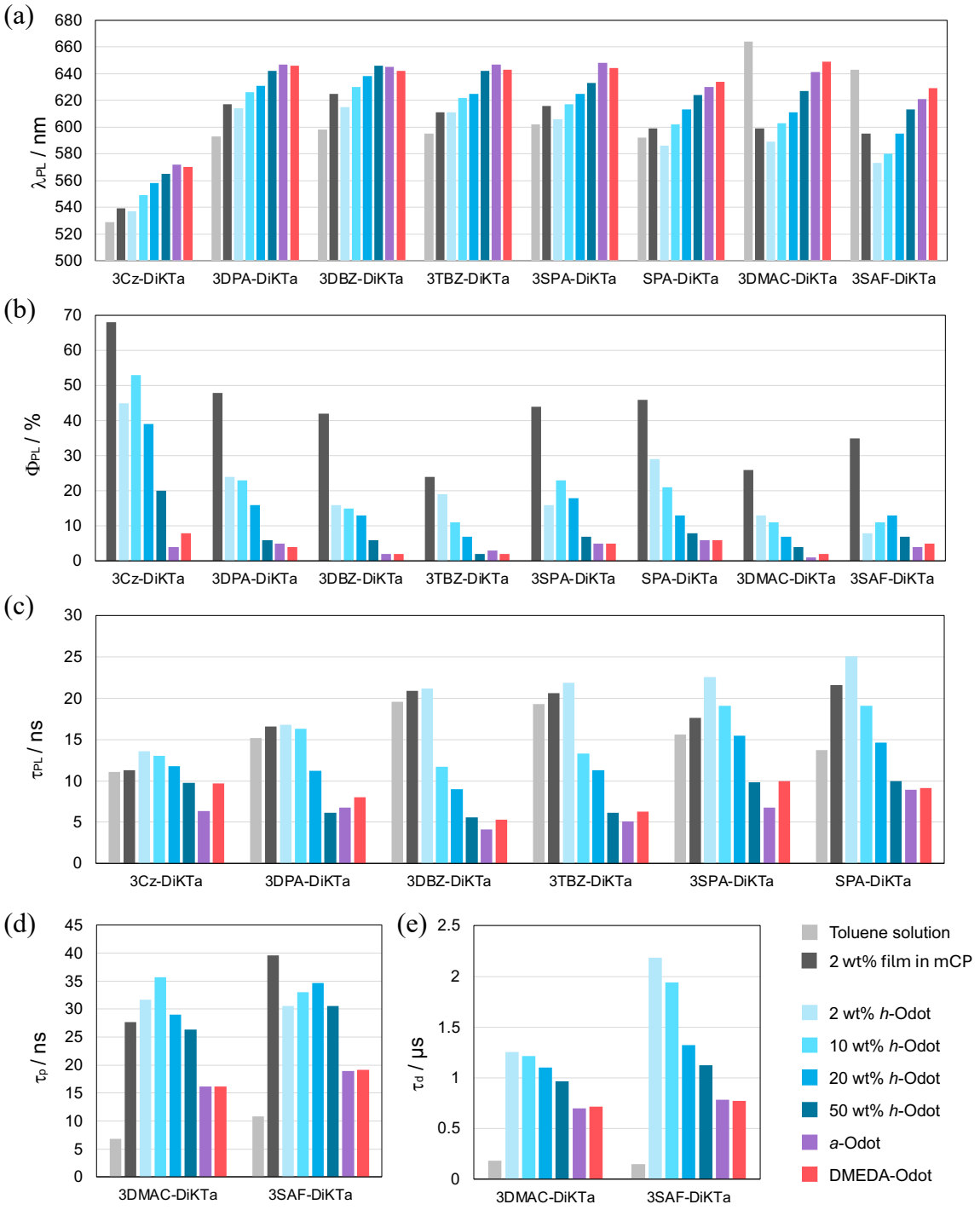


Figure 3. Representation of (a) photoluminescence wavelength λ_{PL}, (b) photoluminescence quantum yields Φ_{PL}, (c) average intensity-weighted mean fluorescence lifetimes, (d) intensity-weighted mean prompt fluorescence lifetimes, and (e) intensity-weighted mean delayed fluorescence lifetimes, of the aqueous Odot solutions. Bars are color-coded by Odot formulation (2, 10, 20, 50 wt% *h*-Odots in shades of blue, *a*-Odots in purple, and DMEDA-containing Odots in red). Lifetimes in dilute toluene solutions (light grey) and 2 wt% mCP films (dark grey) are added for reference.

Structure-Formulation-PL Lifetime Relationships for the TADF Odots

In the context of these promising photophysical results, we evaluated the panel of 48 nanoprobes as FLIM agents in HeLa cells (Figure **4a**). Fluorescence signals were localized intracellularly and within the plasma membrane, as confirmed by Z-stack confocal microscopy (Figure **S37**). Gratifyingly, FLIM images revealed the expected large range of PL lifetimes from the different Odot formulations (Figure **4b**, Figure **S38**–**39**, and Table **S10**). A general trend was observed across the Odots, where the intensity-weighted mean τ_{PL} increased as the propensity for emitter aggregation decreased (i.e., from *a*-Odots to 50 wt% to 2 wt% in the *h*-Odots). The most pronounced changes in τ_{PL} were observed for the families of Odots with trisubstituted emitters with moderate donors. For instance, the τ_{PL} of the Odots of **3DPA-DiKTa** and **3TBZ-DiKTa** increased from 3.6 ns and 4.5 ns as their *a*-Odots to 12.8 ns and 16.3 ns as their 2 wt% *h*-Odots, respectively. The Odots of **SPA-DiKTa** have τ_{PL} of 6–9 ns, a significantly reduced tunability in lifetime compared to **3SPA-DiKTa** (τ_{PL} of 6–13 ns). For all *h*-Odots of **3DMAC-DiKTa** and **3SAF-DiKTa** as well as the 2 wt% *h*-Odots of **3DBZ-DiKTa** and **SPA-DiKTa**, the 10 wt% *h*-Odots of **3DBZ-DiKTa** and the 20 wt% *h*-Odots and DMEDA-Odots of **3TBZ-DiKTa**, low fluorescence intensities were correlated to very short τ_{PL} on the order of that of cellular autofluorescence. Incorporation of the cationic amine DMEDA consistently led to longer PL lifetimes compared to the *a*-Odots. Most DMEDA-Odots showed an average increase of the τ_{PL} of ~4 ns, with the PL lifetime of the Odots of **3DBZ-DiKTa** increasing most dramatically from ~3 ns as *a*-Odots to ~11 ns as DMEDA-Odots. These observations demonstrate that DMEDA is a useful additive to increase the fluorescence lifetimes of Odots.

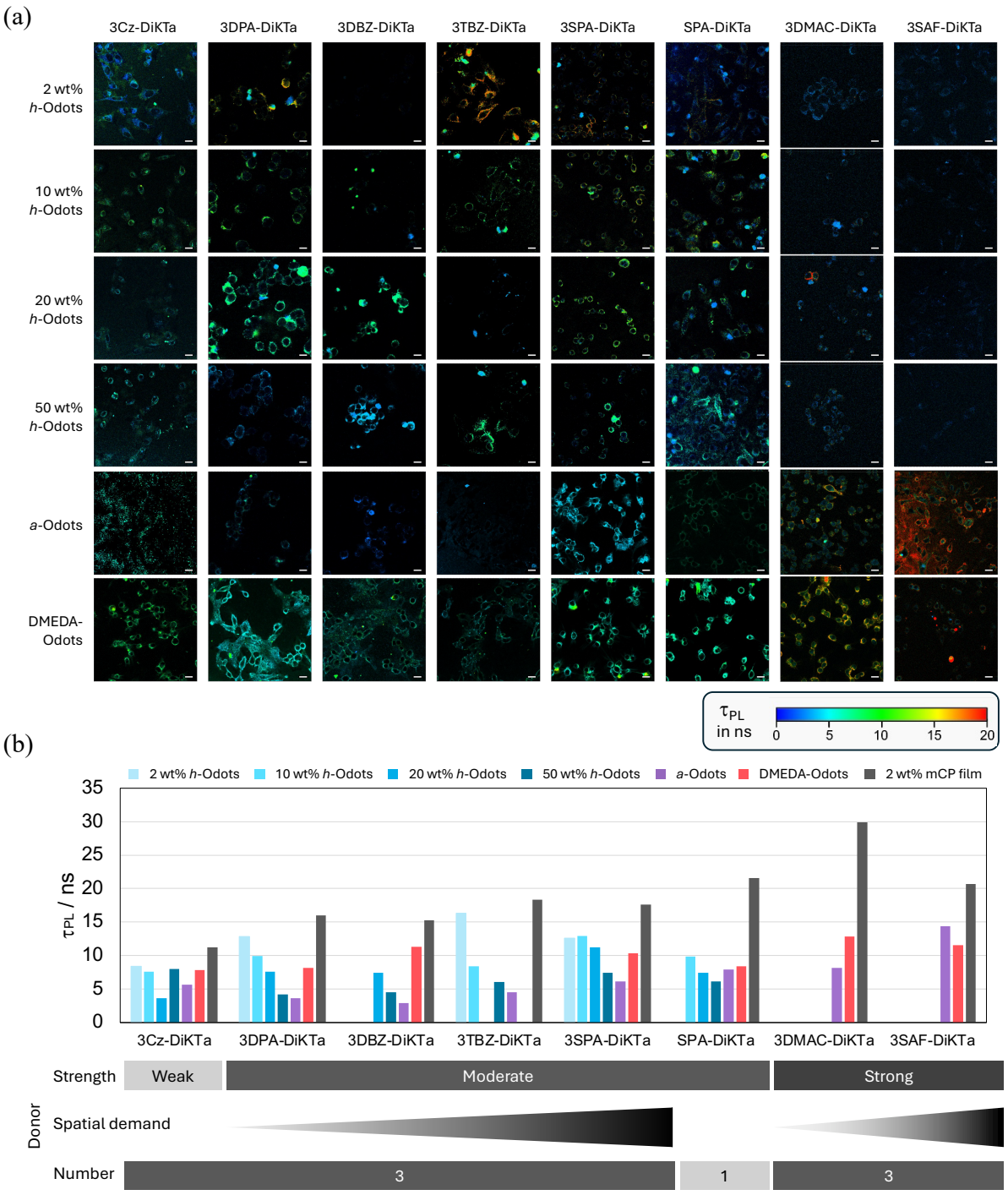


Figure **4**. FLIM images of HeLa cells stained with donor-decorated DiKTa Odots (5 µg mL^{-1}). (a) FLIM maps represent intensity-weighted average lifetimes (τ, ns) on a continuous rainbow scale from 0 ns (blue) to 20 ns (red). Each row corresponds to a different emitter (**SPA-DiKTa, 3SPA-DiKTa, 3Cz-DiKTa, 3TBZ-DiKTa, 3DBZ-DiKTa, 3DPA-DiKTa, 3DMAC-DiKTa,** and **3SAF-DiKTa**), and each column to a distinct nanoprobe formulation: host-containing *h*-Odots with 2, 10, 20, and 50 wt% of emitter in mCP, neat *a*-Odots, and DMEDA-containing Odots. Scale bar: 20 µm. (b) Bar graphs representing the intensity-weighted mean fluorescence lifetimes calculated from fluorescence decay curves fitted using multi-exponential models (10 MHz, 100 ns window). Bars are color-coded by Odot formulation (2, 10, 20, 50 wt% *h*-Odots in shades of blue, *a*-Odots in purple, and DMEDA-containing Odots in red). PL Lifetimes in 2 wt% mCP films (dark grey) are added for reference. Complete decay

curves, fitted lifetime components, and χ^2 values are provided in Figure **S38** and Table **S10**. The trends in donor design are represented beneath.

Systematic characterization of the TADF Odots in *in vitro* assays and live-cell FLIM revealed that both the emitter chemical structure and Odot formulation contribute to modulate the PL lifetimes. First, the co-encapsulation of the emitter with mCP effectively controls the emitter doping and the degree of aggregation, modulating the magnitude of τ_{PL} and the fluorescence intensity, both of which increase at low doping levels of emitter. Second, formulation-dependent lifetime tunability was particularly pronounced for trisubstituted emitters with moderate-strength donors (**3DPA-DiKTa**, **3DBZ-DiKTa**, **3TBZ-DiKTa**, and **3SPA-DiKTa**), where the emitters retain SRCT character and the Odots offer the widest dynamic range in fluorescence lifetime across different formulations. Third, due to the use of strong donors, Odots with **3DMAC-DiKTa** and **3SAF-DiKTa** emit from LRCT states, resulting in lower Φ_{PL} and broad emission bands but longer PL lifetimes than emitters with weaker donors. Furthermore, these emitters feature a significantly increased Stokes shift, requiring high energy excitation, which reduces the compatibility with established FLIM setups. Fourth, the monosubstituted emitter **SPA-DiKTa** emits from a mixed SRCT/LRCT state and the Odots maintain comparable PL lifetimes to the Odots with the trisubstituted emitters, while excitation wavelengths of higher energy are required. Finally, the use of bulky moderate-strength donors (**TBZ** and **SPA**) increases τ_{PL} only by suppressing aggregation at high emitter doping in the nanoparticles. Collectively, these observations demonstrate that structural modification of the **DiKTa** core coupled with formulation enable a wide range of τ_{PL} values and spectral profiles in this family of Odots. On this basis, we selected Odots with **3DPA-DiKTa** to demonstrate the potential of multiplexed FLIM imaging.

Multiplexed FLIM of Co-Cultures of Human Cancer and Immune Cells using a family of Odots with a Single-Emitter

The structure–formulation–lifetime relationships provided a key insight: formulated Odots of different composition based on a single emitter can display a diverse range of emission lifetimes. This property is particularly suited to FLIM-based multiplexing, where discrimination relies not on emission color but also on τ_{PL}. To demonstrate this concept in a biologically meaningful context, we targeted co-cultures of human cancer cells and immune cells as two populations whose spatial organization within the tumor microenvironment influences disease progression.[36] For example, T cells mediate anti-tumor immunity through antigen recognition and cytotoxic signaling, making their visualization alongside cancer cells of considerable diagnostic and mechanistic value.[37, 38] Consequently, imaging agents able to simultaneously image cancer and immune cells are valuable tools to study the tumor microenvironment.

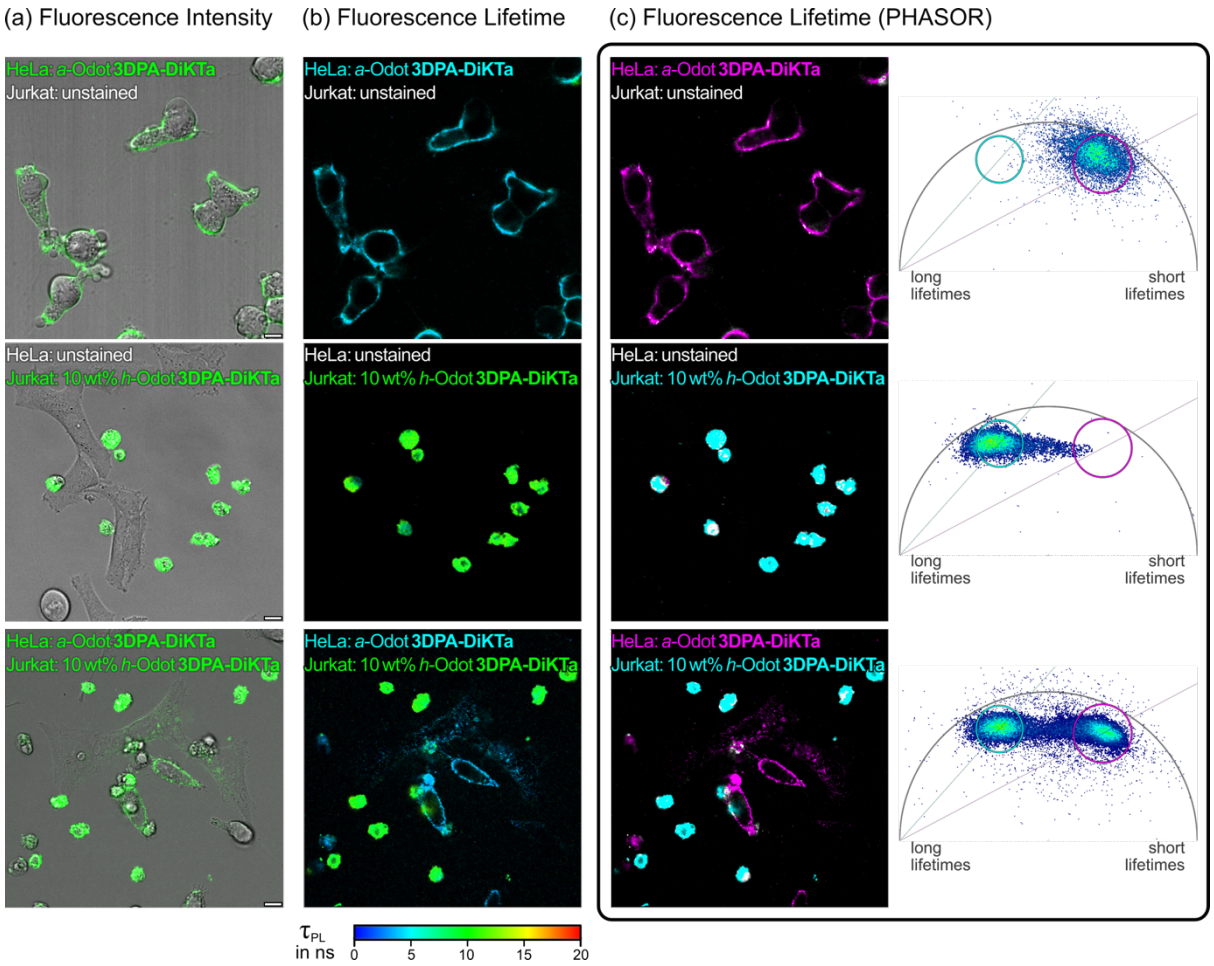


Figure **5**. Lifetime-based multiplexing of cancer and immune cells using a single TADF emitter. (a) Representative fluorescence intensity images (green) overlaid with brightfield of HeLa (cervical cancer) and Jurkat (T lymphocyte) cells labelled with Odots of the same TADF emitter, **3DPA-DiKTa**. Top row: HeLa cells stained with **3DPA-DiKTa** *a*-Odots, with unstained Jurkat cells. Middle row: Jurkat cells stained with **3DPA-DiKTa** 10 wt% *h*-Odots, with unstained HeLa cells. Bottom row: Co-incubated samples containing both pre-stained populations. (b) Corresponding FLIM images (FastFLIM), with intensity-weighted mean fluorescence lifetimes on a continuous color scale from 5 ns (blue) to 20 ns (red). (c) Corresponding FLIM–phasor images and plots. Clusters are color-coded: HeLa (magenta) and Jurkat (cyan). Scale bars: 10 µm.

Therefore, we designed a multiplexed FLIM assay in which different Odot formulations of **3DPA-DiKTa** serve as lifetime-encoded labels to distinguish between cancer and immune cell populations within a single field of view. **3DPA-DiKTa** Odots were selected as they stained HeLa cells with a wide PL lifetime range and emit at between 593–617 nm. HeLa cancer cells were incubated with *a*-Odots, Jurkat T cells were incubated with 10 wt% *h*-Odots of **3DPA-DiKTa** (Figure **5**), and both cell types were co-cultured after washing. Under conventional fluorescence intensity imaging, the two cell types were indistinguishable, that is, both *a*-Odots and 10 wt% *h*-Odots of **3DPA-DiKTa** showed overlapping emission (Figure **5a**). In contrast, FLIM images of the same co-cultures revealed two clearly resolved populations (Figure **5b**, Figure **S40**) as confirmed by FLIM-PHASOR analysis (Figure **5c**). HeLa cancer cells labelled with *a*-Odots showed an average τ_{PL} of approximately 4 ns, while Jurkat T cells stained with 10 wt% *h*-Odots displayed average τ_{PL} of approximately 10 ns, which closely match those obtained

from FLIM experiments with single TADF Odots (Figure **5b** and Figure **4**). This consistency in τ_{PL} confirms that the formulation-encoded lifetime signatures are preserved in the cell co-cultures and are not perturbed by cellular interactions or differential uptake.

These results establish formulation-controlled PL lifetime encoding as a viable multiplexing strategy for biological imaging. This approach circumvents the need for structurally diverse fluorophores, instead exploiting the nanoparticle composition as the sole determinant of contrast in concert with a TADF emitter. Because the underlying emitter remains unchanged, all formulations can be imaged with the same microscopy settings, eliminating the multi-laser configurations and complex filters typically associated with spectral multiplexing. This single-excitation, single-TADF emitter paradigm simplifies the instrumental setup while providing unambiguous cell-type discrimination through the temporal domain. Looking forward, the broad PL lifetime range accessible across the Odot library (4–35 ns) suggests that higher-order multiplexing—encoding three or more cell populations using a single TADF scaffold—is within reach, contingent on sufficient lifetime separation relative to the instrument response function.

Conclusions

We have demonstrated that the PL lifetime of TADF Odots can be tuned through both as a function of the emitter structure and nanoparticle formulation. A library of 48 nanoprobes, built from eight donor-decorated **DiKTa** derivatives across six biocompatible Odot compositions, spans an unprecedented PL lifetime window of 4–35 ns. We identified several structure–formulation–lifetime principles, with the main finding that the PL lifetime is governed primarily by the degree of emitter aggregation within the Odot: doping of the emitter in an mCP host at decreasing doping concentration suppresses quenching, leading to longer τ_{PL} and higher Φ_{PL}, while leaving the absorption profile unchanged. Donor choice sets the dynamic range over which the τ_{PL} can be tuned. Moderate-strength donors preserve the SRCT character of the MR-TADF emitter and their respective Odots and afford the widest formulation-dependent τ_{PL} window and conserves the bright, narrowband emission. The incorporation of strong donors modulates the nature of the excited state to one having significant LRCT character, leading to much longer τ_{PL}. Monosubstituted congeners have excited states of mixed SRCT/LRCT character, while the use of bulky donors leads to emitters with longer τ_{PL} only at high emitter doping levels. Overall, this work demonstrates how PL lifetime can be readily tuned both as a function of TADF emitter design and nanoparticle formulation. Application of these principles *in vitro* confirmed the value of this strategy for bioimaging, with two formulations of a single emitter, **3DPA-DiKTa**, sufficing to discriminate human cancer and immune cells in co-culture by FLIM. These findings demonstrate that rational formulation of Odots of TADF emitters can translate photophysics into a viable imaging tool

for dissecting the cellular heterogeneity of complex biological systems, such as tumor microenvironments.

Acknowledgements

J.H. gratefully acknowledges funding from the Studienstiftung des deutschen Volkes. F.N.B. acknowledges the EPSRC Impact Acceleration Account (EP/X525698/1). We thank the EPSRC (EP/X525819/1, EP/Z535291/1, EP/W007517/1, and EP/W015137/1) for financial support. The authors acknowledge support by the state of Baden-Württemberg through bwHPC and the German Research Foundation (DFG) through grant no INST 40/575-1 FUGG (JUSTUS 2 cluster). We acknowledge funding for SEM from the EPSRC via EP/R023751/1 and EP/T019298/1. DBC acknowledge support for the St Andrews Single-Crystal X-Ray Diffraction Service from an EPSRC Core Equipment Grant (UKRI381) and the University of St Andrews Strategic Equipment Fund. The authors thank Dr. Euan Kay for kindly granting us access to his Zetasizer and Dr. Aaron Naden for performing the SEM experiments. We also acknowledge Pilar Suárez de Cepeda for technical support with initial imaging experiments. The authors thank Dr. Oliver Lee and Dr. Qianyu Cai for technical support with calcualtions.

Author Contributions

CRediT: J.H.: conceptualization, data curation, formal analysis, investigation, methodology, visualization, writing - original draft, writing - review & editing. F.N.-B.: conceptualization, data curation, formal analysis, investigation, methodology, visualization, writing - original draft, writing - review & editing. A.J.: investigation, data curation, writing – review & editing. D.B.C.: formal analysis, investigation, writing – review & editing. A.P.M.: formal analysis, investigation. O.F.: formal analysis, investigation, writing – review & editing. M.V.: conceptualization, funding acquisition, methodology, project administration, resources, supervision, writing – review & editing. S.B.: funding acquisition, project administration, resources, supervision, writing – review & editing. E.Z.-C.: conceptualization, funding acquisition, methodology, project administration, resources, supervision, writing – review & editing.

Supporting Information

Synthetic procedures, ^{1}H NMR and ^{13}C NMR spectra, HRMS and IR spectra, computational data and coordinates, crystallographic data, supplementary photophysical, and biological data.

Data Availability Statement

The research data supporting this publication can be accessed at https://dx.doi.org/10.14272/collection/JAH_2025-08-18. CCDC 2529806 and 2554036-2554038 contain the supplementary crystallographic data. These data can be obtained free of charge from The Cambridge Crystallographic Data Centre via www.ccdc.cam.ac.uk/structures.

Conflict of Interest

The authors declare that a patent application has been filed related to the work described in this manuscript. Marc Vendrell and Eli Zysman-Colman are listed as inventors. Patent application number: 2600356.6.

References

(1) Andreou, C.; Weissleder, R.; Kircher, M. F. Multiplexed imaging in oncology. *Nat. Biomed. Eng.* **2022**, *6* (5), 527-540.
(2) Torrado, B.; Pannunzio, B.; Malacrida, L.; Digman, M. A. Fluorescence lifetime imaging microscopy. *Nat. Rev. Methods Primers* **2024**, *4* (1), 80.
(3) Berezin, M. Y.; Achilefu, S. Fluorescence lifetime measurements and biological imaging. *Chem. Rev.* **2010**, *110* (5), 2641-2684.
(4) Lim, C.; Seah, D.; Vendrell, M. Chemical fluorophores for fluorescence lifetime imaging. *Chem. Soc. Rev.* **2026**, *55* (3), 1352-1370.
(5) Zhang, K. Y.; Yu, Q.; Wei, H.; Liu, S.; Zhao, Q.; Huang, W. Long-Lived Emissive Probes for Time-Resolved Photoluminescence Bioimaging and Biosensing. *Chem. Rev.* **2018**, *118* (4), 1770-1839.
(6) Dos Santos, J. M.; Basumatary, B.; Bryden, M.; Chen, D.; Choudhary, P.; Comerford, T.; Crovini, E.; Danos, A.; De, J.; Diesing, S.; et al. The golden age of thermally activated delayed fluorescence materials: design and exploitation. *Chem. Rev.* **2024**, *124* (24), 13736-14110.
(7) Madayanad Suresh, S.; Hall, D.; Beljonne, D.; Olivier, Y.; Zysman‐Colman, E. Multiresonant thermally activated delayed fluorescence emitters based on heteroatom‐doped nanographenes: recent advances and prospects for organic light‐emitting diodes. *Adv. Funct. Mater.* **2020**, *30* (33), 1908677.
(8) Yuan, Y.; Tang, X.; Du, X. Y.; Hu, Y.; Yu, Y. J.; Jiang, Z. Q.; Liao, L. S.; Lee, S. T. The design of fused amine/carbonyl system for efficient thermally activated delayed fluorescence: novel multiple resonance core and electron acceptor. *Adv. Opt. Mater.* **2019**, *7* (7), 1801536.
(9) Guo, Z.; Zhang, X.; Zhou, A.; Utochnikova, V.; Zhu, Y.; Meng, H. Chemical Strategies for Modifying Carbonyl/Nitrogen‐Based MR‐TADF Materials toward Narrowband Emission. *Adv. Opt. Mater.* **2025**, *13* (28), e01289.
(10) Wu, S.; Li, W.; Yoshida, K.; Hall, D.; Madayanad Suresh, S.; Sayner, T.; Gong, J.; Beljonne, D.; Olivier, Y.; Samuel, I. D. W. Excited-state modulation in donor-substituted multiresonant thermally activated delayed fluorescence emitters. *ACS Appl. Mater. Interfaces* **2022**, *14* (19), 22341-22352.
(11) Ni, F.; Zhu, Z.; Tong, X.; Zeng, W.; An, K.; Wei, D.; Gong, S.; Zhao, Q.; Zhou, X.; Yang, C. Hydrophilic, Red-Emitting, and Thermally Activated Delayed Fluorescence Emitter for Time-Resolved Luminescence Imaging by Mitochondrion-Induced Aggregation in Living Cells. *Adv. Sci.* **2019**, *6* (5), 1801729.
(12) Zhang, Q.; Xu, S.; Li, M.; Wang, Y.; Zhang, N.; Guan, Y.; Chen, M.; Chen, C.-F.; Hu, H.-Y. Rationally designed organelle-specific thermally activated delayed fluorescence small molecule organic probes for time-resolved biological applications. *Chem. Commun.* **2019**, *55* (39), 5639-5642.
(13) Xu, S.; Zhang, Q.; Han, X.; Wang, Y.; Wang, X.; Nazare, M.; Jiang, J.-D.; Hu, H.-Y. Dual-Mode Detection of Bacterial 16S Ribosomal RNA in Tissues. *ACS Sens.* **2020**, *5* (6), 1650-1656.
(14) Zhang, J.; Chen, R.; Zhu, Z.; Adachi, C.; Zhang, X.; Lee, C.-S. Highly Stable Near-Infrared Fluorescent Organic Nanoparticles with a Large Stokes Shift for Noninvasive Long-Term Cellular Imaging. *ACS Appl. Mater. Interfaces* **2015**, *7* (47), 26266-26274.
(15) Zhang, J.; Chen, W.; Kalytchuk, S.; Li, K. F.; Chen, R.; Adachi, C.; Chen, Z.; Rogach, A. L.; Zhu, G.; Yu, P. K. N.; et al. Self-Assembly of Electron Donor–Acceptor-Based Carbazole Derivatives: Novel Fluorescent Organic Nanoprobes for Both One- and Two-Photon Cellular Imaging. *ACS Appl. Mater. Interfaces* **2016**, *8* (18), 11355-11365.
(16) Zhang, J.; Fang, F.; Liu, B.; Tan, J.-H.; Chen, W.-C.; Zhu, Z.; Yuan, Y.; Wan, Y.; Cui, X.; Li, S.; et al. Intrinsically Cancer-Mitochondria-Targeted Thermally Activated Delayed Fluorescence Nanoparticles for Two-Photon-Activated Fluorescence Imaging and Photodynamic Therapy. *ACS Appl. Mater. Interfaces* **2019**, *11* (44), 41051-41061.

(17) Wei, R.; Zhang, L.; Xu, S.; Zhang, Q.; Qi, Y.; Hu, H.-Y. A single component self-assembled thermally activated delayed fluorescence nanoprobe. *Chem. Commun.* **2020**, *56* (17), 2550-2553.
(18) Hu, W.; Guo, L.; Bai, L.; Miao, X.; Ni, Y.; Wang, Q.; Zhao, H.; Xie, M.; Li, L.; Lu, X.; et al. Maximizing Aggregation of Organic Fluorophores to Prolong Fluorescence Lifetime for Two-Photon Fluorescence Lifetime Imaging. *Adv. Healthc. Mater.* **2018**, *7* (15), 1800299.
(19) He, T.; Ren, C.; Li, Z.; Xiao, S.; Li, J.; Lin, X.; Ye, C.; Zhang, J.; Guo, L.; Hu, W.; et al. Thermally activated delayed fluorescence organic dots for two-photon fluorescence lifetime imaging. *Appl. Phys. Lett.* **2018**, *112* (21), 211102.
(20) Li, T.; Yang, D.; Zhai, L.; Wang, S.; Zhao, B.; Fu, N.; Wang, L.; Tao, Y.; Huang, W. Thermally Activated Delayed Fluorescence Organic Dots (TADF Odots) for Time-Resolved and Confocal Fluorescence Imaging in Living Cells and In Vivo. *Adv. Sci.* **2017**, *4* (4), 1600166.
(21) Xu, S.; Wei, R.; Chen, Z.; Ma, P.; Qiang, G.; Peng, H.; Hu, H.-Y. Lipid droplet formation and dynamics: tracking by time-resolved fluorescence imaging. *Mater. Chem. Front.* **2022**, *6* (24), 3691-3697.
(22) Zhu, Z.; Tian, D.; Gao, P.; Wang, K.; Li, Y.; Shu, X.; Zhu, J.; Zhao, Q. Cell-Penetrating Peptides Transport Noncovalently Linked Thermally Activated Delayed Fluorescence Nanoparticles for Time-Resolved Luminescence Imaging. *J. Am. Chem. Soc.* **2018**, *140* (50), 17484-17491.
(23) Tsuchiya, Y.; Ikesue, K.; Nakanotani, H.; Adachi, C. Photostable and highly emissive glassy organic dots exhibiting thermally activated delayed fluorescence. *Chem. Commun.* **2019**, *55* (36), 5215-5218.
(24) Primrose, W. L.; Sevilla-Pym, A.; Hudson, Z. M. The Future is Bright: The Emergence of Glassy Organic Dots for Biological Applications. *Chem. Eur. J.* **2025**, *31* (1), e202403399.
(25) de Cepeda, P. S.; Nadal‐Bufi, F.; Haug, J.; Matulaitis, T.; Zhou, Y.; Lochenie, C.; Qi, Q.; Jung, A.; Chen, D.; González‐Bello, C. Biocompatible TADF probes for highly multiplexed fluorescence lifetime imaging. *Angew. Chem. Int. Ed.* **2026**, e21482.
(26) Fang, F.; Zhu, L.; Li, M.; Song, Y.; Sun, M.; Zhao, D.; Zhang, J. Thermally Activated Delayed Fluorescence Material: An Emerging Class of Metal-Free Luminophores for Biomedical Applications. *Adv. Sci.* **2021**, *8* (24), 2102970.
(27) Xia, Y.; Zheng, M.; Li, X.; Song, K.; Teng, Z. Enhancing biological imaging with high-performance probes based on thermally activated delayed fluorescence. *iScience* **2025**, *28* (10).
(28) Mayder, D. M.; Christopherson, C. J.; Primrose, W. L.; Lin, A. S.; Hudson, Z. M. Polymer dots and glassy organic dots using dibenzodipyridophenazine dyes as water-dispersible TADF probes for cellular imaging. *J. Mater. Chem. B* **2022**, *10* (34), 6496-6506.
(29) Masvikeni, T. R.; Primrose, W. L.; Mikulin, S.; Hudson, Z. M. Water-Dispersible Glassy Organic Dots Exhibiting Near-Infrared Delayed Emission for Bioimaging. *ACS Appl. Nano Mater.* **2025**, *8* (23), 11856-11864.
(30) Qiu, X.; Jung, A.; Sevilla-Pym, A.; Hu, P.; Bräse, S.; Hudson, Z. M. Glassy organic dots exhibiting near-infrared TADF with quantum yields > 40% for cellular imaging. *J. Mater. Chem. B* **2025**, *13* (41), 13282-13288.
(31) Mamada, M.; Aoyama, A.; Uchida, R.; Ochi, J.; Oda, S.; Kondo, Y.; Kondo, M.; Hatakeyama, T. Efficient Deep-Blue Multiple-Resonance Emitters Based on Azepine-Decorated ν-DABNA for CIEy below 0.06. *Adv. Mater.* **2024**, *36* (30), 2402905.
(32) Wu, S.; Kumar Gupta, A.; Yoshida, K.; Gong, J.; Hall, D.; Cordes, D. B.; Slawin, A. M.; Samuel, I. D.; Zysman‐Colman, E. Highly Efficient Green and Red Narrowband Emissive Organic Light‐Emitting Diodes Employing Multi‐Resonant Thermally Activated Delayed Fluorescence Emitters. *Angew. Chem. Int. Ed.* **2022**, *61* (52), e202213697.
(33) Hall, D.; Sancho-García, J. C.; Pershin, A.; Ricci, G.; Beljonne, D.; Zysman-Colman, E.; Olivier, Y. Modeling of Multiresonant Thermally Activated Delayed Fluorescence Emitters—Properly Accounting for Electron Correlation Is Key! *J. Chem. Theory Comput.* **2022**, *18* (8), 4903-4918.
(34) Lee, O.S.; Zysman-Colman, E. Digichem (version 7) Chemicus Limited, St Andrews, Scotland, 2025.
(35) Lee, O. S.; Gather, M. C.; Zysman-Colman, E. Digichem: computational chemistry for everyone. *Digital Discovery* **2024**, *3* (9), 1695-1713.

(36) Bruni, D.; Angell, H. K.; Galon, J. The immune contexture and Immunoscore in cancer prognosis and therapeutic efficacy. *Nat. Rev. Cancer* **2020**, *20* (11), 662-680.
(37) Wang, X.; Barrera, C.; Bera, K.; Viswanathan, V. S.; Azarianpour-Esfahani, S.; Koyuncu, C.; Velu, P.; Feldman, M. D.; Yang, M.; Fu, P.; et al. Spatial interplay patterns of cancer nuclei and tumor-infiltrating lymphocytes (TILs) predict clinical benefit for immune checkpoint inhibitors. *Sci. Adv. 8* (22), eabn3966.
(38) Oliveira, G.; Wu, C. J. Dynamics and specificities of T cells in cancer immunotherapy. *Nat. Rev. Cancer* **2023**, *23* (5), 295-316.

TOC

